Vis Comput (2010) 26: 555–563
DOI 10.1007/s00371-010-0459-5

ORIGINAL ARTICLE

Realistic rendering of bokeh effect based on optical aberrations

Jiaze Wu · Changwen Zheng · Xiaohui Hu · Yang Wang · Liqiang Zhang

Published online: 14 April 2010

Abstract Bokeh effect is an important characteristic for realistic image synthesis. However, existing bokeh rendering methods are incapable of simulating realistic bokeh effects due to not taking into account optical characteristics of real lenses, especially optical aberrations. In this paper, a novel realistic bokeh rendering method, based on an accurate camera lens model and distributed ray tracing, is presented. An optical analysis of the relationship between bokeh and optical aberrations, including spherical aberration, coma, astigmatism and field curvature, is firstly introduced. Based on this analysis, a physically-based camera lens model, which takes detailed lens prescription as input, is then introduced for accurately modeling the aberrations. The position and diameter of the entrance and exit pupils are calculated by tracing rays inside the lens for achieving efficient ray sampling, and a general sequential ray tracing algorithm is proposed to better combine with bidirectional ray tracing. Furthermore, correct integration between the lens model and bidirectional ray tracing is also analyzed. The rendering results demonstrate a variety of realistic bokeh effects caused by the aberrations.

Keywords Bokeh effect · Optical aberrations · Realistic rendering · General sequential ray tracing

J. Wu (✉) · C. Zheng · X. Hu · Y. Wang · L. Zhang
Institute of Software, Chinese Academy of Sciences, Beijing, China
e-mail: wujiaze05@gmail.com

J. Wu · Y. Wang · L. Zhang
Graduate University of Chinese Academy of Sciences, Beijing, China

1 Introduction

Bokeh refers to the appearance of the circle of confusion (COC) for an out-of-focus (OOF) point, especially for small or point light sources, and highlights in out-of-focus areas of a photo [1, 19]. Bokeh often appears in photos produced by large-aperture lenses, macro lenses, and long telephoto lenses because they are typically used with a shallow depth of field (DOF). Different lenses produce different bokeh effects in the background or foreground of photos, and these effects vary in the COC shape and light intensity distribution in the COC depending on optical characteristics of lenses. Lens manufacturers, including Nikon, Canon, and Minolta, provide some lenses, which are deliberately designed to capture bokeh more easily for photographers. With these lenses, photographers introduce a variety of bokeh effects in their artistic works for reducing distractions of viewers, emphasizing primary subject and enhancing sense of art of an image.

For a computer-synthesized image, bokeh effect can enhance realism and improve depth perception and user comprehension. Therefore, a number of methods have been proposed to add bokeh into synthesized images, but none of them produce accurate bokeh effect due to lack of accurate lens model. Motivated by this observation, a new method for rendering realistic bokeh effect is proposed in this paper. Our method firstly introduces a new physically-based lens model, which is generalization of Kolb's lens model [12]. The lens model is implemented based on accurate geometrical description of real lenses and law of refraction. As a result, the optical properties of real lenses are accurately modeled and the bokeh appearance, including the COC shape and the light intensity distribution within the COC, truly reflect the aberrations existing in lenses. Furthermore, the accurate lens model and distributed ray tracing technique are combined in support of rendering realistic bokeh effect.

2 Related work

2.1 Depth-of-field rendering

Bokeh effect is closely related with DOF effect because DOF effect refers to blurring in OOF areas, and can be considered as a simplified case of bokeh effect under a thin lens. Plenty of DOF rendering methods have been developed, forming a spectrum of quality-performance trade-off, from accurate to fast techniques. These methods can be divided into two groups: multi-pass methods [4, 9, 17, 21, 26] and post-processing methods [13, 14, 16, 18, 22, 24, 30]. The multi-pass methods can achieve most accurate DOF effect at heavy computational cost, while the post-processing methods are mainstream for rendering DOF effect at interactive rate at the cost of loss of reality. However, all those methods are only capable of simulating DOF effect produced by the thin lens model, and incapable of obtaining more complicated DOF effect (namely bokeh effect) caused by complicated real lenses.

2.2 Bokeh rendering

As bokeh effect can be viewed as complicated DOF effect, many rendering methods for DOF effect can be extended to render bokeh effect. According to wave optics and thin lens model, Potmesil and Chakravarty [22] derived the Lommel function to describe the intensity distribution in the COC, but did not propose and implement any algorithm for producing bokeh effect of real lenses.

Riguer et al. [23] presented a gathering-based method for rendering bokeh effect, and applied a number of filters with different shapes and intensity distributions to obtain diverse effects. Kodama et al. [11] proposed a similar method, but exploited multiplication operation in frequency domain instead of convolution operation in spatial domain for accelerating rendering process. However, Kass et al. [10] pointed out that rendering relatively high-quality bokeh effect with gathering methods is rather difficult, since bokeh patterns are determined by the scattered pixels from a source image rather than the gathered neighbor pixels.

Lee et al. [16] proposed a scattering-based method for simulating more accurate bokeh for defocused highlights. This method easily renders the effect by exploiting texture extension of GPU point sprites. Lanman et al. [15] modeled various shapes of COC by compositing a set of simple images describing basic aperture shapes. Based on summed area table technique, Kosloff et al. [13] implemented a variety of effects of different shapes and intensity distributions.

All these methods above are based on image post-processing techniques, and only generate approximate effect. Buhler et al. [3] proposed a bokeh rendering method based on distributed ray tracing, where an arbitrary probability density function is specified to represent the light intensity distribution within the COC. This method achieves more accurate effect than post-processing methods, but only uses the thin lens model.

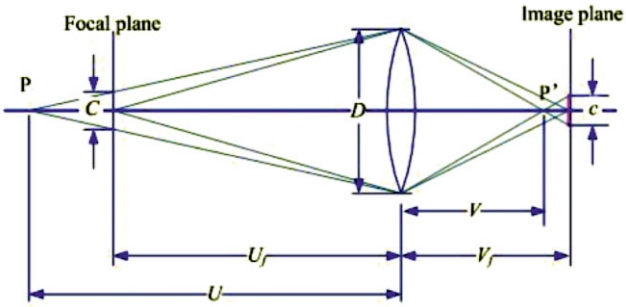

Fig. 1 Basic optical principle of bokeh effect: the formation of the COC

3 Circle of confusion

In this section, we begin with the formation of the COC to explain basic idea of bokeh effect. Figure 1 illustrates a thin lens with the focal length, f, and the aperture diameter, D. Any point on the focal plane can be sharply focused on the image plane. However, for an out-of-focus point, its images on the image plane will be a blur disk, which is often called circle of confusion.

To calculate the diameter of the COC, we first give two important equations according to the lens equation [7]:

$$V_f = \frac{U_f f}{U_f - f},$$

$$m = \frac{V_f}{U_f},$$

where U_f is the distance from the focal plane to the lens, also called focal distance, V_f is the distance from the image plane to the lens, and m is the magnification. Using the similar triangle theory, the diameter, C, of blur disk on the focal plane produced by P can be represented as

$$C = D\frac{|U - U_f|}{U},$$

where U is the distance from P to the lens, also called object distance. Finally, the diameter of the COC on the image plane is obtained by multiplying the magnification m by C:

$$c = mC = \frac{|U - U_f|V_f}{U_f U} D = \frac{|U - U_f|f}{U(U_f - f)} D. \quad (1)$$

As seen from (1), the diameter of the COC depends on the aperture size, focal length, object distance, and focal distance, and thereby these factors determine whether bokeh effect can appear in out-of-focus areas. In a thin lens model,

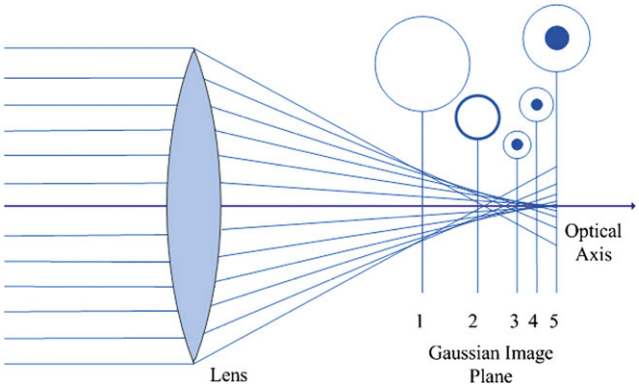

Fig. 2 A simple lens with negative spherical aberration. The marginal rays have a shorter focal length than the central rays

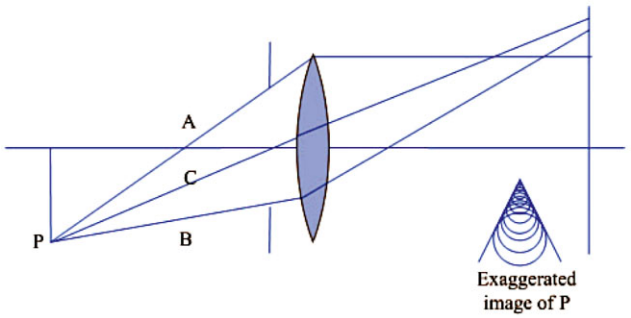

Fig. 3 In the presence of coma, the rays through the periphery of the lens are focus at a different height than the rays through the center of the lens

the COC is always assumed to be circular and uniformly distributed, as adopted by DOF rendering methods. However, in a real lens system, the COC is often non-circular due to optical aberrations, and the light intensity distribution in the COC varies with different real lenses because of their optical aberrations. In next section, we give an optical analysis about the impact of optical aberrations on the COC shape and the light intensity distribution within the COC.

4 Optical aberrations

Optical aberrations, ubiquitous in real lens systems, refer to departure of the imaging performance of a lens system from the perfect prediction by Gaussian optics [2]. Optical aberrations lead to blurring of images, and affect the appearance of bokeh effect, including its shape and intensity distribution. In this section, we will analyze how various kinds of optical aberrations affect bokeh on images.

4.1 Spherical aberration

Most lenses are composed of spherical surfaces due to low manufacture cost, but their shape is not ideal for the formation of a sharp image and leads to spherical aberration. This is because that the refracted light rays have different focal lengths when they strike a lens near the periphery in comparison with those near the center of the lens. Spherical aberration can be considered as a kind of on-axis aberration because it only occurs for an on-axis point.

Figure 2 illustrates the spherical aberration of a single lens. Notice that the light rays that hit the lens close to the optical axis are focused at position 5, far from the lens but very near the Gaussian focus. As the ray height hitting the lens increases, the position of the intersection with the optical axis moves closer and closer to the lens (for example, positions 4, 3, 2, and 1). When the periphery focus is located farther from the lens than the Gaussian focus, the lens is considered to suffer from positive spherical aberration. Conversely, the lens features negative spherical aberration, which is the case for the lens in Fig. 2.

Depending on how a lens is corrected for spherical aberration, the COC of an axial out-of-focus point may be uniformly illuminated, brighter near the edge, brighter near the center, or even some kind of more complex form. In Fig. 2, the COC at position 5 is characterized by a bright core surrounded by faint halo, whereas the COC at position 1 has a darker core surrounded by a bright ring of light. Such anomalous light distributions often appear in the out-of-focus parts of a photograph, and popular among portrait photographers for their artistic sense.

4.2 Coma

Coma (also called comatic aberration) refers to the distortion of the image for an off-axis point. Therefore, coma is considered a kind of off-axis aberration compared to spherical aberration. When a beam of oblique rays hits a lens with coma, the rays passing through the edge of the lens may be focused at a different height from those passing through the center and the difference in height is called comatic aberration. As illustrated in Fig. 3, the upper and lower marginal rays, A and B, intersect the image plane below the ray C passing through the center of the lens. Coma usually affects the COC shape, and the appearance of the image formed by a comatic lens is indicated in the right-bottom side of Fig. 3. Obviously, which features the comet shape in accord with the name of the aberration.

4.3 Astigmatism and field curvature

Ideally, a lens system captures a 3D scene onto a flat image plane, where a digital sensor or film lies. However, this is not the case for the image formation in practice, and deviation from a flat image plane always occurs because of astigmatism and field curvature. In the presence of astigmatism, an off-axis point will have two different sharp images,

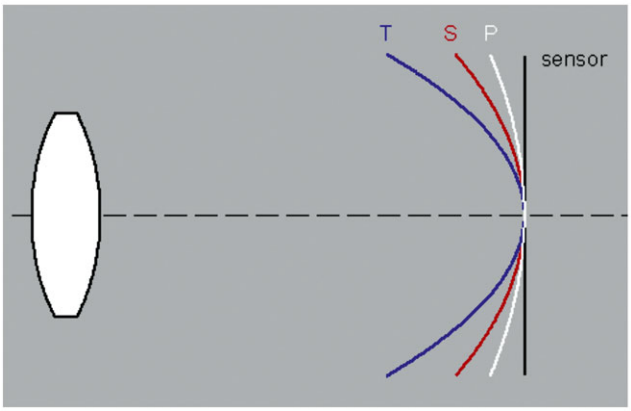

Fig. 4 A simple lens with undercorrected astigmatism. T = tangential surface; S = sagittal surface; P = Petzval surface. Image courtesy of Paul van Walree [29]

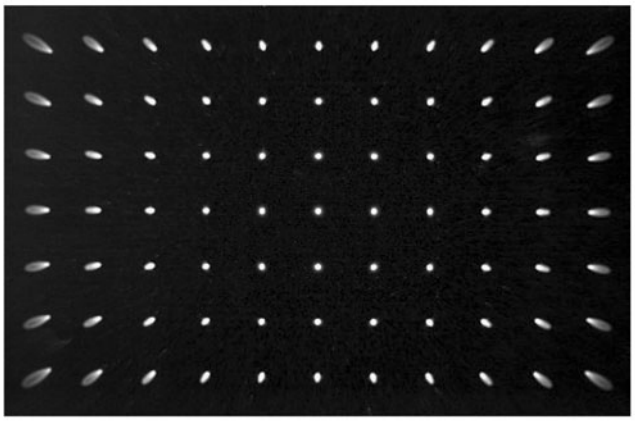

Fig. 5 Bokeh effect of a grid of white dots produced by a lens with astigmatism and field curvature. (Planar 1.4/50 at F/1.4 and the central dot in focus.) Image courtesy of Paul van Walree [29]

namely tangential and sagittal images, at different positions. All tangential and sagittal images in the field of view form tangential and sagittal image surfaces, respectively, for example surfaces T and S shown in Fig. 4. In the absence of astigmatism, the tangential and sagittal image surfaces will coincide, and form a single surface, called Petzval surface, such as surface P shown in Fig. 4.

Astigmatism and field curvature have an important impact on the shape of bokeh. For an off-axis point, when its tangential image moves away from its Gaussian focus, its real image will be elongated in sagittal (or radial) direction; when its sagittal image moves away from its Gaussian focus, its real image will be elongated in tangential direction. Figure 5 illustrates bokeh effect produced by a lens with astigmatism and field curvature in Fig. 4. The elongation of the COCs towards the image corners can be directly attributed to the astigmatism and field curvature in Fig. 4. Since the tangential image surface is further away from the Gaussian image plane than the sagittal image surface, the COCs will be blurred more in radial direction. The blur shapes in Fig. 5, which are mainly due to astigmatism, should not be confused with the blur shape of a lens that suffers from coma (Sect. 4.2).

5 Rendering of bokeh effect

5.1 A physically-based lens model

5.1.1 Law of refraction

The law of refraction, also called Snell law, is a formula used to describe the relationship between the angles of incidence and refraction when light passes through a boundary between two different transparent materials. Lens elements are made of transparent materials, such as glass, plastic, and crystalline, and therefore the law of refraction can be exploited to describe the behavior of light through a lens system. For convenience of ray tracing calculation, the law of refraction is denoted in a vector form,

$$n(\mathbf{I} \times \mathbf{N}) = n'(\mathbf{T} \times \mathbf{N}),$$

where $\mathbf{I}$ and $\mathbf{T}$ are the unit vectors of the incident and refracted rays, respectively, $\mathbf{N}$ is the unit vector of the normal at the intersection between the incident ray and the lens surface, and n and n' are the indices of refraction of both materials, respectively. The law can be rewritten as

$$\left(\mathbf{T} - \frac{n}{n'}\mathbf{I}\right) \times \mathbf{N} = 0,$$

which indicates that $\mathbf{T} - \frac{n}{n'}\mathbf{I}$ and $\mathbf{N}$ have the same or inverse direction, and therefore we obtain

$$\mathbf{T} - \frac{n}{n'}\mathbf{I} = \Gamma\mathbf{N},$$

where Γ is called partial derivative. Giving dot product for both side of the equation, we obtain

$$\Gamma = \mathbf{T} \cdot \mathbf{N} - \frac{n}{n'}\mathbf{I} \cdot \mathbf{N} = \cos\theta' - \frac{n}{n'}\cos\theta$$
$$= \sqrt{1 - \frac{n^2}{n'^2}\left(1 - (\mathbf{I} \cdot \mathbf{N})^2\right)} - \mathbf{I} \cdot \mathbf{N},$$

where θ and θ' are respectively the angles of incidence and refraction. Hence, the unit vector of the refracted ray can be denoted as

$$\mathbf{T} = \frac{n}{n'}\mathbf{I} + \Gamma\mathbf{N}. \quad (2)$$

Equation (2) can be used to calculate the direction of the refracted ray in general sequential ray tracing algorithm inside a lens system.

5.1.2 Calculation of entrance and exit pupils

When tracing rays passing through a lens system, a naive ray sampling method is connecting two points sampled on the image plane and the rear lens, which is closest to the image plane. However, this method is fairly low in efficiency because majority of the rays that pass through the rear lens are blocked by the rims of lens elements, and cannot pass through the entire lens system, shown in the profile view of the first lens in Fig. 6.

In order to improve the efficiency of the ray sampling, we exploit the optical properties of the aperture stop and its pupils, shown in Fig. 6. The aperture stop is the aperture that most limits the amount of light entering a lens system, the entrance pupil represents the image of the aperture stop when viewed from the object space, and the exit pupil the image from the image space [7]. There is a conjugate relationship among aperture stop, entrance and exit pupils for a lens system. In others words, if a ray from a point passes through either of them, it also passes other ones and finally passes through the entire lens system. Conversely, if the ray cannot pass through any of them, it cannot also pass through any others. Therefore, only sampling rays between the image plane and exit pupil can improve the efficiency of the ray tracing, especially when the diameter of the aperture stop is small compared to the other apertures in the lens system, as shown in the profile views of the second and third lenses of Fig. 6.

Based on the optical properties among the aperture stop and its pupils, an algorithm for locating the pupils and calculating their diameters is presented. This algorithm can be divided into two steps: first, the positions of the pupils are calculated by ray tracing; second, the diameters of the pupils are determined using Gaussian optics [7] and ray tracing. The detailed process about the algorithm is shown as follows:

Step 1 Point P_0 is initialized as the center of the object (image) plane, $P_{\min}$ as the center of the front (rear) lens, and $P_{\max}$ as the marginal point of the front (rear) lens;

Step 2 Assuming the ray $R_{\min}$ from P_0 to $P_{\min}$, the ray $R_{\max}$ from P_0 to $P_{\max}$, and the ray R_1 equal to $R_{\max}$;

Step 3 If the difference between the directional cosines of $R_{\min}$ and $R_{\max}$ is not less than the specified minimum value and the number of iteration is not more than the maximum value specified in advance, continue the following steps; Otherwise, return to Step 5;

Step 4 Forward (backward) trace the ray R_1. If the ray R_1 can pass through the lens system, $R_{\min} = R_1$; Otherwise $R_{\max} = R_1$. Then $R_1 = (R_{\min} + R_{\max})/2$, return to Step 3;

Step 5 The ray R_1 is namely the marginal ray of the entrance (exit) pupil;

Step 6 The point P_0 is initialized as the center of the aperture stop, and the point P_3 as the paraxial point on the optical lens before (after) the aperture stop;

Step 7 Let ray R_2 from P_0 to P_3, and backward (forward) trace the ray R_2 until it goes out of the lens system;

Step 8 The position of the center of the entrance (exit) pupil is namely the intersection of R_2 and the optical axis, and diameter of the entrance (exit) pupil is determined by its position and the marginal ray R_1. The algorithm ends.

5.1.3 General sequential ray tracing inside the lens

Since all lens elements of a lens system can be stored into a data structure in a sequence of light ray path, consequently ray tracing inside the lens system can proceed in sequence. Furthermore, the support for backward and forward ray tracing inside the lens system is also needed for integration into a general ray tracer. Therefore we present a general sequential approach for tracing rays inside the lens system from its front or rear. Compared to the traditional distributed ray tracing algorithm, the ray tracing inside the lens system need not to find the closest intersection and avoid heavy computation of sorting and intersection, and therefore the efficiency for tracing is fairly high. When the general sequential ray tracing algorithm is integrated into a general ray tracing renderer, an accurate camera lens model will be introduced to simulate the optical properties of a real lens but the performance of the renderer does not decrease too much. When rendering a complex 3D scene, the ray tracing in the 3D scene takes up nearly majority of the rendering time and the ray tracing inside the lens system rarely contributes to the rendering time. The detailed process of the algorithm is described as follow:

Step 1 Generate a ray R from P_1 to P_2, where P_1 and P_2 are sample points on the image plane (3D scene) and exit pupil (or entrance pupil), respectively;

Step 2 Iterate each lens element in the lens system. If there are any elements, compute the intersection P_0 of the ray R and the element, continue following steps; Otherwise, return to Step 5;

Step 3 If P_0 is beyond the aperture of the element, the ray R is blocked and cannot pass through the element, and the algorithm ends; Otherwise the ray R can pass through the element, continue the following steps;

Step 4 Compute the normal N of the element at P_0. Compute the refracted ray T. Then update R using T using (2), return to Step 2;

Step 5 R is namely the ray shooting from the lens system, and the algorithm ends.

5.2 Ray Tracing in a 3D scene

There are three representative ray tracing approaches, namely path tracing, light tracing and bidirectional path tracing [28], for solving the light transport equation in a 3D scene. Since bidirectional path tracing can be considered as a combina-

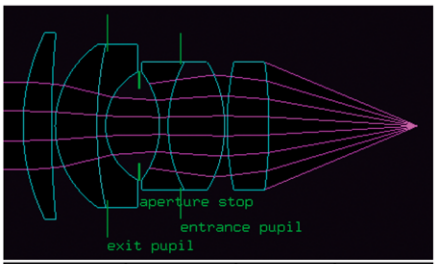

radius	thickness	index	aperture
85.500	11.600	1.744	76.0
408.330	1.500	1.000	76.0
40.350	17.000	1.620	66.0
156.050	3.500	1.621	66.0
25.050	13.700	1.000	44.0
0.000	8.300	1.000	42.6
-36.800	3.500	1.689	44.0
55.000	23.000	1.744	52.0
-51.500	1.000	1.000	52.0
123.500	17.000	1.744	52.0
-204.960	0.000	1.000	52.0

(a) F/1.35

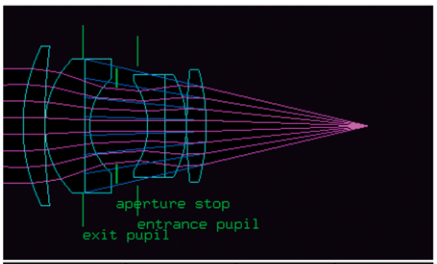

radius	thickness	index	aperture
75.050	9.000	1.717	66.0
270.700	0.100	1.000	66.0
39.270	16.510	1.667	55.0
0.000	2.000	1.673	55.0
25.650	10.990	1.000	39.0
0.000	13.000	1.000	37.2
-31.870	7.030	1.673	37.0
0.000	8.980	1.717	42.0
-43.510	0.100	1.000	42.0
221.140	7.980	1.667	46.0
-88.790	0.000	1.000	46.0

(b) F/1.7

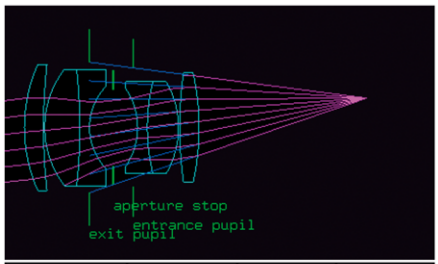

radius	thickness	index	aperture
93.900	7.900	1.611	52.0
240.300	0.500	1.000	52.0
39.500	14.500	1.623	48.0
-220.500	4.000	1.606	48.0
24.500	9.950	1.000	34.0
0.000	9.950	1.000	31.8
-28.700	4.000	1.606	32.0
78.800	12.900	1.623	38.0
-37.900	0.500	1.000	38.0
161.900	8.000	1.623	45.0
-103.200	0.000	1.000	45.0

(c) F/2.0

Fig. 6 Profile view and tabular description of three double Gauss lenses with a focal length 100 mm [25]: from *left* to *right*, the lenses are F/1.35, F/1.7 and F/2.0. Each row in the *tables* describes a surface of a lens element. Surfaces are listed in order from front to rear, with basic measurement unit in millimeters. The *first column* gives the signed radius of a spherical surface; if 0.0 is given, the surface is planar. A positive radius indicates a surface that is convex when viewed from the front of the lens, while a negative radius indicates a concave surface. The *next entry* is thickness, which measures the distance from this surface to the next surface along the optical axis. Following that is the index of refraction at the sodium d line (587.6 nm) of the material between the surface and the next surface. If 1.0 is given, the material is assumed to be air. The *last entry* is the diameter of the aperture of the surface. The *row* with a radius of 0.0 and air at both sides of the surface signifies an adjustable diaphragm, namely the aperture stop

tion of path tracing and light tracing, we will only figure how the physically-based lens model is integrated into bidirectional path tracing.

Bidirectional path tracing connects two subpaths, namely camera subpath and light subpath, to obtain the advantages of both path tracing and light tracing. When the lens model proposed in this paper is integrated into bidirectional path tracing, some modifications to this tracing method need be taken to realize the correct integration between them. Moreover, the integration into path tracing and light tracing is similar the treatment on camera and light subpaths, respectively.

Camera subpath. When generating a camera subpath, the first vertex of the subpath should be placed at the entrance pupil for easily connecting a light subpath. If the vertex is placed at the exit pupil for conveniently generating rays between the image plane and the camera, the connection between the vertex and a light subpath will be impossible. However, the corresponding conjugate vertex on the exit pupil is also exploited to sample a new ray between the image plane and the exit pupil. The new ray is traced inside the lens system to obtain a ray leaving the lens system. The exitant ray is assigned to the first vertex of the eye subpath for calculating next vertex.

Light subpath. When a light subpath is connected to a camera subpath of only one vertex, a new ray between two subpaths is generated. The new ray starts on the entrance pupil of a lens system, and determine the position of the image plane which the combined path contribute to. The ray tracing process inside the lens system is necessary to obtain the position of the image plane. However, if the computed position is beyond the image plane, the combined path will be discarded.

6 Results and discussion

Our rendering method is implemented to produce realistic and artistic bokeh effect. All results were rendered on a 3.0G Intel Xeon 5450, with three double Gauss lenses, shown in Fig. 6.

Figure 7 shows bokeh effects produced by a tiny light source using three lenses for five different focal distances. In Fig. 7(a), when the focal distance is 1000 mm, no bokeh comes because the light source is in focus and has a sharpest image. As the focal distance increases or decreases, the image of the light source begins to become larger and more blurring and bokeh begins to appear. When the focal distance is less than 1000 mm, the image is a dark circle with a

bright thin ring, for example at focal distances 800 mm and 900 mm. When the focal distance is more than 1000 mm, the image is a bright core with a dark ring, but the bright core has a dark center, as shown at focal distances 1100 mm and 1200 mm. In Fig. 7(b), the changes of the light intensity are similar to the first row except that there is a slightly bright core in the dark circle at focal distance 900 mm. In Fig. 7(c), the changes of the light intensity are greatly different from the former two rows. The image is a uniform circle for the focal distance 800 mm, a bright core surrounded by a dark thick ring for the focal distances 900 mm, and a dark circle surrounded by a bright ring for the focal distances 1100 mm and 1200 mm. Note that the size of the COCs varies with the focal distance, as explained in Sect. 3. The changes of the light intensity distribution due to the focal distance are attributed to the change of the spherical aberration with the focal distance. Different lenses can produce different bokeh effects at the same focal distance because they have different spherical aberrations.

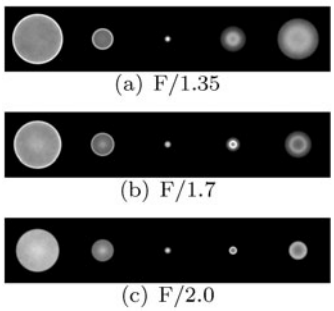

Fig. 7 A tiny light source at a distance of 1000 mm from the lens used and in the center of the field of view of the lens. From top row to bottom row, the lenses used are F/1.35, F/1.7 and F/2.0. From left column to right column, the focal distances are 800 mm, 900 mm, 1000 mm, 1100 mm and 1200 mm. Note that bokeh effects vary with different lenses and focal distances

Figure 8 show bokeh effects of the highlights on a row of balls using three lenses at five focal distances. For the balls in the center, their highlights have circular COCs when defocused, and various intensity distributions within the COCs, which are only dependent on the spherical aberration of the lenses used. However, as with the balls close to the edge, the COCs begin to become non-circular and are characterized by a variety of shapes, such elliptical and cometic, and light intensity distributions within the COCs are more complex than that of balls in the center. The shape and intensity distribution are determined by coma, astigmatism and field curvature, as is explained in Sect. 4. Figure 9 shows

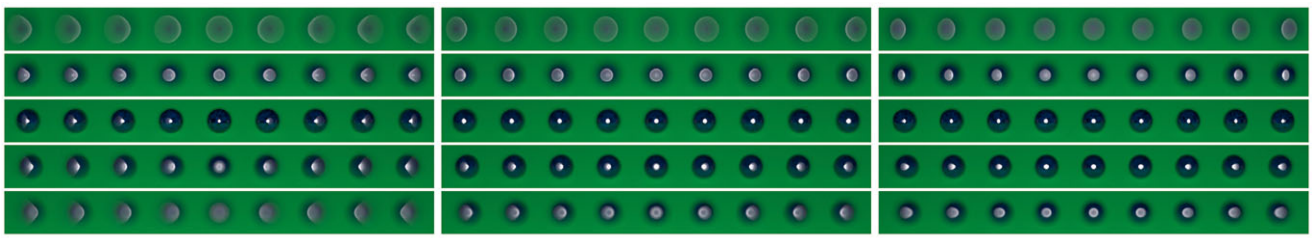

Fig. 8 A row of balls for showing bokeh effect using the lenses, F/1.35, F/1.7 and F/2.0, at different focal distances. Note that the changes of bokeh effects from center to edge due the focal distances and optical aberrations

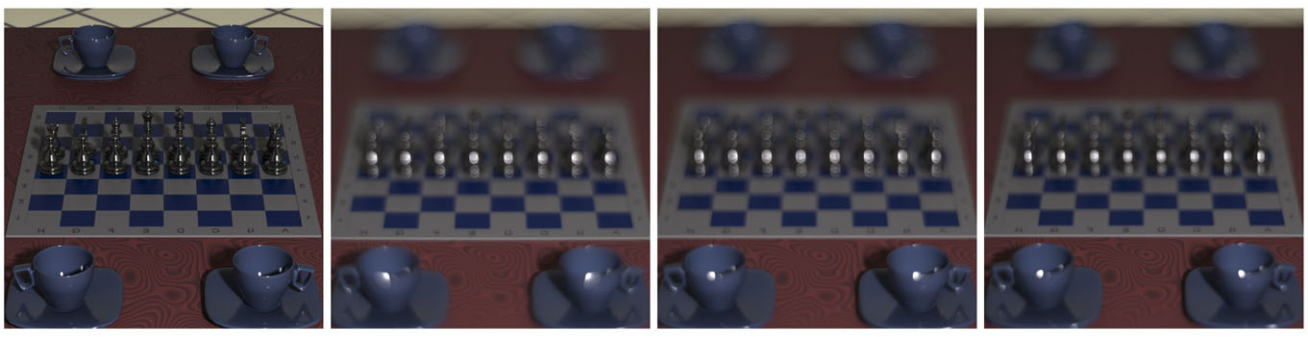

Fig. 9 A chess scene for showing bokeh effects using the pinhole lens and three lenses, F/1.35, F/1.7 and F/2.0

bokeh effect in a slightly complex chess scene, from which we can see various bokeh effects due to optical aberrations in both foreground and background of each image similar to Fig. 8.

7 Conclusion

In this paper, the influence of the optical aberrations on the shape and light intensity distribution of bokeh effects has been analyzed. In order to simulate these aberration-based effects, an accurate camera lens model, which exploits the lens parameters of real lenses, has been introduced. General sequential ray tracing inside the lens model, in support of backward and forward ray tracing, has been presented for better integration with bidirectional path tracing. An algorithm for obtaining the position and aperture size of the entrance and exit pupils of a lens system has been proposed, and the pupils are utilized for more efficiently guiding ray sampling. For correct integration between the lens model and bidirectional path tracing, the way to select the first vertex of a camera subpath has been analyzed. Moreover, general sequential ray tracing inside the lens model has been exploited to generate light and camera subpaths. In summary, with all above techniques, optical aberrations of real lenses are accurately simulated and corresponding bokeh effects have been also synthesized.

An important issue of future work is to analyze and synthesize bokeh effects due to aperture shape, vignetting and chromatic aberrations, and generalize our method to rendering more effects. Spectral rendering techniques [5, 6, 27] would be required since chromatic aberrations are caused by the variation of the index of refraction with the wavelength. Adaptive sampling techniques [8, 20, 26] would be combined with our methods to accelerate rendering of bokeh effects.

Acknowledgements We would like to very thank Yuxuan Zhang, Jie Zhang and Chao Li for their valuable comments. We also thank the LuxRender community and the chess model creators. This work was partly supported by the National High-Tech Research and Development Plan of China (Grant No. 2009AA01Z303).

References

1. Ang, T.: Dictionary of Photography and Digital Imaging: The Essential Reference for the Modern Photographer. Watson-Guptill, New York (2002)
2. Born, M., Wolf, E.: Principles of Optics, 7 edn. Cambridge University Press, Cambridge (1999)
3. Buhler, J., Wexler, D.: A phenomenological model for bokeh rendering. In: Computer Graphics Proceedings, Annual Conference Series, ACM SIGGRAPH Abstracts and Applications, p. 142. San Antonio (2002)
4. Cook, R.L., Porter, T., Carpenter, L.: Distributed ray tracing. In: Computer Graphics Proceedings, Annual Conference Series, ACM SIGGRAPH, pp. 137–145. Minneapolis (1984)
5. Devlin, K., Chalmers, A., Wilkie, A., Purgathofer, W.: Tone reproduction and physically based spectral rendering. In: Eurographics 2002: State of the Art Reports, pp. 101–123 (2002)
6. Evans, G.F., McCool, M.D.: Stratified wavelength clusters for efficient spectral Monte Carlo rendering. In: Graphics Interface, pp. 42–49 (1999)
7. Fischer, R.E., Tadic-Galeb, B., Yoder, P.R.: Optical System Design, 2nd edn. McGraw-Hill, New York (2008)
8. Hachisuka, T., Jarosz, W., Weistroffer, R.P., Dale, K.: Multidimensional adaptive sampling and reconstruction for ray tracing. ACM Trans. Graph. (SIGGRAPH 08) **27**(3), 33 (2008)
9. Haeberli, P., Akeley, K.: The accumulation buffer: Hardware support for high-quality rendering. In: Computer Graphics Proceedings, Annual Conference Series, ACM SIGGRAPH, pp. 309–318. Dallas (1990)
10. Kass, M., Lefohn, A., Owens, J.: Interactive depth of field using simulated diffusion on a gpu. Technical report, Pixar Animation Studios (2006)
11. Kodama, K., Mo, H., Kubota, A.: Virtual bokeh generation from a single system of lenses. In: Computer Graphics Proceedings, Annual Conference Series, ACM SIGGRAPH Research Posters, p. 77. Boston (2006)
12. Kolb, C., Mitchell, D., Hanrahan, P.: A realistic camera model for computer graphics. In: Computer Graphics Proceedings, Annual Conference Series, ACM SIGGRAPH, pp. 317–324. Los Angeles (1995)
13. Kosloff, T.J., Tao, M.W., Barsky, B.A.: Depth of field postprocessing for layered scenes using constant-time rectangle spreading. In: Proceedings of Graphics Interface, pp. 39–46. Kelowna (2009)
14. Kraus, M., Strengert, M.: Depth-of-field rendering by pyramidal image processing. Comput. Graph. Forum **26**(3) (2007)
15. Lanman, D., Raskar, R., Taubin, G.: Modeling and synthesis of aperture effects in cameras. In: Proceedings of International Symposium on Computational Aesthetics in Graphics, Visualization, and Imaging, pp. 102–106. Lisbon (2008)
16. Lee, S., Kim, G.J., Choi, S.: Real-time depth-of-field rendering using point splitting on per-pixel layers. Comput. Graph. Forum **27**(7), 1955–1962 (2008)
17. Lee, S., Eisemann, E., Seidel, H.P.: Depth-of-field rendering with multiview synthesis. ACM Trans. Graph. (Proc. ACM SIGGRAPH ASIA) **28**(5), 1–6 (2009)
18. Lee, S., Kim, G.J., Choi, S.: Real-time depth-of-field rendering using anisotropically filtered mipmap interpolation. IEEE Trans. Vis. Comput. Graph. **15**(3), 453–464 (2009)
19. Merklinger, H.M.: A technical view of bokeh. Photo Tech. **18**(3), 37–41 (1997)
20. Overbeck, R.S., Donner, C., Ramamoorthi, R.: Adaptive wavelet rendering. ACM Trans. Graph. (SIGGRAPH Asia 09) **28**(5), 140 (2009)
21. Pharr, M., Humphreys, G.: Physically Based Rendering: From Theory to Implementation. Morgan Kaufmann, San Francisco (2004)
22. Potmesil, M., Chakravarty, I.: A lens and aperture camera model for synthetic image generation. In: Computer Graphics Proceedings, Annual Conference Series, ACM SIGGRAPH, pp. 297–305. Dallas (1981)
23. Riguer, G., Tatarchuk, N., Isidoro, J.: Real-time depth of field simulation. In: Engel, W.F. (ed.) Shader X2: shader programming tips and tricks with DirectX 9, pp. 529–556. Wordware, Plano (2003)
24. Rokita, P.: Fast generation of depth-of-field effects in computer graphics. Comput. Graph. **17**(5), 593–595 (1993)
25. Smith, W.J.: Modern Lens Design. McGraw Hill, New York (1992)

26. Soler, C., Subr, K., Durand, F., Holzschuch, N., Sillion, F.: Fourier depth of field. ACM Trans. Graph. **28**(2), 18 (2009)
27. Sun, Y., Fracchia, F.D., Drew, M.S., Calvert, T.W.: A spectrally based framework for realistic image synthesis. Vis. Comput. **17**(7), 429–444 (2001)
28. Veach, E.: Robust Monte Carlo methods for light transport simulation. Ph.D. thesis, Stanford University (1997)
29. van Walree, P.: Astigmatism and field curvature. URL http://toothwalker.org/optics/astigmatism.html
30. Zhou, T., Chen, J., Pullen, M.: Accurate depth of field simulation in real time. Comput. Graph. Forum **26**(1), 15–23 (2007)

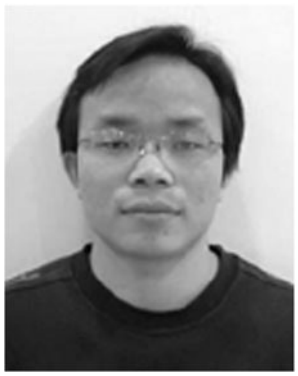

Jiaze Wu is a Ph.D. student in the National Key Laboratory of Integrated Information System Technology, Institute of Software, Chinese Academy of Sciences. He received his B.Sc. degree from Nankai University in 2005. His research interests include real-time rendering, realistic rendering, virtual reality and optical simulation.

Changwen Zheng is a Professor in the National Key Laboratory of Integrated Information System Technology, Institute of Software, Chinese Academy of Sciences. He received his Ph.D. degree from Huazhong University of Science and Technology. His research interests include computer graphics, virtual reality, computer simulation and artificial intelligence.

Xiaohui Hu is a Professor in the National Key Laboratory of Integrated Information System Technology, Institute of Software, Chinese Academy of Sciences. He received his Ph.D. degree from Beijing University of Aeronautics and Astronautics. His research interests include computer graphics, virtual reality and computer simulation.

Yang Wang is a Ph.D. student in the National Key Laboratory of Integrated Information System Technology, Institute of Software, Chinese Academy of Sciences. His research interests include real-time rendering, realistic rendering and 3D modeling.

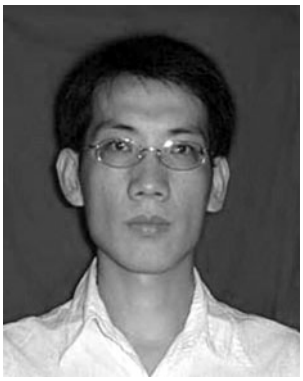

Liqiang Zhang is a Ph.D. student in the National Key Laboratory of Integrated Information System Technology, Institute of Software, Chinese Academy of Sciences. His research interests include real-time rendering, realistic rendering, virtual reality and atmosphere simulation.